RL-TR-95-287
Final Technical Report
February 1996

OPTICAL INTERCONNECT/PROCESSING METHODS FOR PARALLEL ACCESS OPTICAL MEMORY

Rockwell Science Center

John Hong

APPROVED FOR PUBLIC RELEASE; DISTRIBUTION UNLIMITED.

Rome Laboratory
Air Force Materiel Command
Rome, New York

This report has been reviewed by the Rome Laboratory Public Affairs Office (PA) and is releasable to the National Technical Information Service (NTIS). At NTIS, it will be releasable to the general public, including foreign nations.

RL-TR-95-287 has been reviewed and is approved for publication.

APPROVED: Paul L. Repak

PAUL L. REPAK
Project Engineer

FOR THE COMMANDER: Gary D. Barmore

GARY D. BARMORE, Major, USAF
Deputy Director of Surveillance & Photonics

If your address has changed or if you wish to be removed from the Rome Laboratory mailing list, or if the addressee is no longer employed by your organization, please notify Rome Laboratory/ (OCPC), Rome NY 13441. This will assist us in maintaining a current mailing list.

Do not return copies of this report unless contractual obligations or notices on a specific document require that it be returned.

REPORT DOCUMENTATION PAGE

Form Approved
OMB No. 0704-0188

1. AGENCY USE ONLY (Leave Blank)	2. REPORT DATE	3. REPORT TYPE AND DATES COVERED
	February 1996	Final Dec 91 - Apr 95

4. TITLE AND SUBTITLE

OPTICAL INTERCONNECT/PROCESSING METHODS FOR PARALLEL ACCESS OPTICAL MEMORY

5. FUNDING NUMBERS

C - F30602-92-C-0012
PE - 62702F
PR - 4519
TA - 21
WU - 95

6. AUTHOR(S)

John Hong

7. PERFORMING ORGANIZATION NAME(S) AND ADDRESS(ES)

Rockwell Science Center
1049 Camino Dos Rios
Thousand Oaks CA 91360

8. PERFORMING ORGANIZATION REPORT NUMBER

N/A

9. SPONSORING/MONITORING AGENCY NAME(S) AND ADDRESS(ES)

Rome Laboratory/OCPC
25 Electronic Pky
Rome NY 13441-4515

10. SPONSORING/MONITORING AGENCY REPORT NUMBER

RL-TR-95-287

11. SUPPLEMENTARY NOTES

Rome Laboratory Project Engineer: Paul L. Repak/OCPC/(315) 330-3146

12a. DISTRIBUTION/AVAILABILITY STATEMENT

Approved for public release; distribution unlimited.

12b. DISTRIBUTION CODE

13. ABSTRACT (Maximum 200 words)

This report summarizes the progress, accomplishments, and status of our effort on the study of optical methods for parallel access optical memory. The main objectives of this project are to develop important optical amplification techniques to increase optical enery efficiency and novel optical interconnection and/or processing techniques to increase the versatility of new parallel access optical memory concepts. The goal is to relieve the electronic cache bottleneck and help realize high net data transfer rates.

14. SUBJECT TERMS

Optical computing, Optical interconnects

15. NUMBER OF PAGES

48

16. PRICE CODE

17. SECURITY CLASSIFICATION OF REPORT	18. SECURITY CLASSIFICATION OF THIS PAGE	19. SECURITY CLASSIFICATION OF ABSTRACT	20. LIMITATION OF ABSTRACT
UNCLASSIFIED	UNCLASSIFIED	UNCLASSIFIED	UL

Table of Contents

List of Figures

1.0 Summary

1.1 Background

Although developments in computers with the emergence of parallel and supercomputers have been nothing short of dramatic, they have not kept pace with the ever-increasing demands placed by signal processing, scientific computing and database computing applications. With the gate switching speeds now in the GHz range (with GaAs technology, for example), the trend has been to opt for parallel computing architectures to increase the processing throughput, with several such machines boasting processing speeds in the 1 GFlop (10^9 floating point operations per second) range.

One particularly prominent weakness in the contemporary machines is the long-term memory. Although the magnetic disk, by far the most commonly used long-term storage technology, offers very high data storage densities, it suffers from a slow memory access speed due to its limited parallelism. Even with the multiple disk approach, a limited number of bits at a time can be read out at a given instant of time. For example, the data transfer rate even for high performance disk systems such as that found in the latest multiple platter disk systems for image processing lies in the 10 MByte/sec. In contrast, optical memory such as volume holographic memory and certain specially configured disk memories offer a high degree of parallel access that is not possible with magnetic disks. This inherent parallel access allows an entire page of 10^4 Bytes to be dumped simultaneously onto a detector/cache memory in 1 microsecond or less (the time needed for the detector/cache to respond to the light), resulting in an effective data transfer rate of 10 GBytes/sec. The detector/cache is a detector array where each pixel coincides with a memory location and the array is configured as a random access memory (RAM). Using parallel access, the *raw* data transfer rate can thus easily be improved by over three orders of magnitude.

Such improvements in memory access performance are not without drawbacks, however. One problem stems from the fact that once the optical information is transferred onto the cache memory, any electronic processing of data before it reaches the CPU gives rise to a *net* transfer rate that is rather slow (electronic cache bottleneck). While such processing is best done in *parallel* while the information is still in the optical format to maintain a high *net* transfer rate, the low optical energy efficiency with which information is accessed in optical memory systems using either volume or planar media necessitates implementation of an optical amplification technique.

1.2 Program Objectives and Goal

The main objectives of this project are to develop important optical amplification techniques to increase the optical energy efficiency and novel optical interconnection/processing techniques to increase the versatility of new parallel access optical memory concepts. The final goal is to relieve the electronic cache bottleneck and help to realize high *net* data transfer rates.

1.3 Progress and Accomplishments

Highlights of the progress and accomplishments in this program include:

- Experimental demonstration of volume holographic content addressable optical memory system
- Sensitivity Measurement of Photorefractive Optical Amplifier Based on Two-Beam Coupling
- Demonstration of a high-speed, high-gain photorefractive amplifier
- Development of a theoretical model and the experiment verification of fanning noise in photorefractive amplifier
- Demonstration of a reconfigurable optical image switching/routing system

Incorporation of a photorefractive optical amplifier in a parallel access holographic memory system can improve the optical energy efficiency. Consequently, the flexibility of using various parallel processing techniques (such as optical image routing discussed in Sections 2.3 and 3.5) while the data are still in the optical domain is enhanced. The combination of these techniques can thus relieve the electronic cache bottleneck and increase the net data transfer rate.

2.0 Technical Discussion

2.1 Volume Holographic Optical Memory

The concept of storing data in the form of multiplexed holographic gratings in volume media had been proposed during the sixties [1–3] and developed with limited success, limited primarily by the immaturity of the required optical and optoelectronic component technologies. The fundamental idea underlying a variety of holographic storage strategies that are known is the recording of a large number of complex holograms in a common volume of holographic material and subsequently spatially multiplexing such common volume storage units to build up the required storage capacity [4]. Each object beam that is spatially modulated with data (page) is recorded with a reference beam. Bragg selectivity provided by the volume interaction allows independent retrieval of each stored page on the basis of optical parameters such as the wavelength, the angle of arrival of the reference beam or the spatial phase distribution of the reference wave. Such techniques have been demonstrated, but they achieved limited performance with respect to capacity and data transfer rate because of the relatively immature material and component technologies that were available at that time [4-6].

With recent advances in the growth and preparation of holographic materials along with the maturation of associated device technologies such as spatial light modulators and detector arrays, the realization of working memory systems that are capable of delivering required performance levels for long-term storage applications is now becoming feasible. For example, the numerous electronic imaging applications that are driven by a large and diverse consumer market have produced relatively low-cost, high-performance detector arrays that can be used for the holographic data storage application. Also, the flat panel display businesses are continuing to improve the resolution, speed, contrast performance and cost-effectiveness for liquid crystal display panels that can also serve as the spatial light modulators required for recording data holographically.

The reemerging interest in the use of holography has been, in part, encouraged by many new developments and demonstrations in multiplex holography and associated techniques. The successful storage of 500 high resolution, angularly multiplexed holograms in $LiNbO_3$ by Mok et al. [9] sparked renewed interest in holographic data storage, followed by more recent results that have demonstrated the storage and recall of up to 10,000 complex image-bearing holograms superposed in relatively small volumes (e.g., on the order of 1 cm^3) [10–12]. The understanding of the various multiplexing options has been upgraded by numerous analyses and experiments that explored issues such as crosstalk and dynamic range [13–18]. The peculiarities of photorefractive

media and their impact on the system design have resulted in proposals for dual wavelength operation to overcome the volatility caused by photorefractive erasure [19]. The same issue was studied from the material perspective, and both thermal and electrical fixing methods were explored [20-22] to determine which method would transform the light-sensitive photorefractive gratings into nonvolatile holograms that do not decay with further light exposure. Another recent development in holographic memories is the introduction of digital error correction techniques to demonstrate sufficiently low bit error rates to allow highly reliable digital data storage [7,8].

The necessary components of a holographic mass memory system are shown in the simplified diagram of Fig. 1. A laser supplies the necessary object and reference beams for both the recording (data storage) and the reconstruction (data retrieval) processes. A spatial light modulator (SLM) spatially encodes the object beam with a page of data to be recorded. Depending on the particular common-volume multiplexing technique that is used, the reference beam is either directed at a particular angle (angular multiplexing) or spatially phase modulated (phase code multiplexing) to serve as the proper page address. In the case of wavelength multiplexing, the addressing mechanism is provided by wavelength selection, which must be provided by a tunable laser. For data retrieval, a properly addressed reference beam (angle of arrival, spatial phase distribution or wavelength) illuminates the holographic storage medium yielding an optical reconstruction of the associated page of data. The reconstructed page is converted into an electronic data pattern via a detector array. The interface between the mass memory system and external users is also important and must include error correction coding [7,8] for the data loaded into the SLM during recording and decoding circuitry for the electronic data pattern emerging from the detector array.

The configuration depicted in Fig. 1 can function as a content addressable memory (CAM) system with very minor modification. In a CAM system, a partial content of a page (rather than a specific page address) is provided to the system as an input in the readout phase. The beam carrying the partial information is diffracted by the holographic storage medium into a set of correlation signal beams (or spots). Whereas the position of each spot uniquely defines the address of a specific page, the intensity of each represents the degree of similarity between the input and each stored page of information. After proper detection, thresholding, and simple processing of the correlation signals, the addresses of those pages containing the query can be derived. This information is then used to position the beam-forming device so that the pages containing the input query are read out page by page. In summary, a CAM system essentially links the two stages (namely, the recording and the readout) to form a closed loop operation. Our progress on volume holographic CAM system demonstration is discussed in Section 3.1.

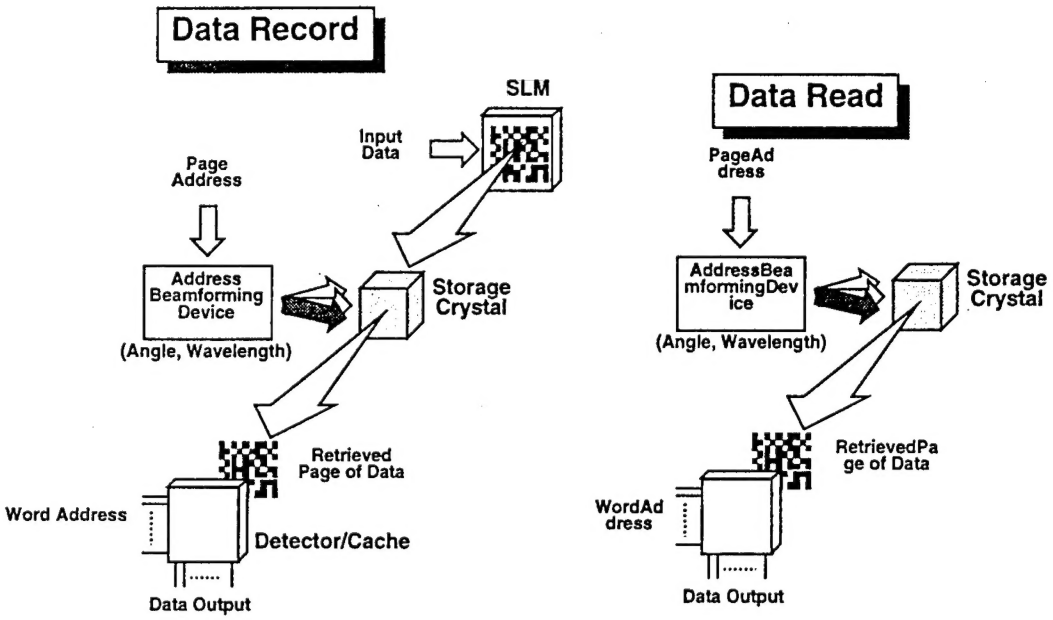

Fig. 1 Simplified System Diagram of Holographic Mass Memory.

2.2 Photorefractive Optical Amplifier for Readout Signal Amplification

2.2.1 Amplified Memory Readout System

A major task to be studied both theoretically and experimentally in this program is the use of photorefractive two-wave mixing for amplification of the weak signal beams that are read out of holographic or disk-based memories. The problem of energy efficiency arises in the case of disk memory because in magnetooptic and other technologies based on phase transitions of materials, the modulation depth of each recorded bit of information is small [23]. The same is true for volume holographic memories where angularly multiplexed holograms are used to store pages of data within the same volume so that a plane wave directed into the medium along a certain orientation reconstructs the desired page of information. Here, the finite dynamic range of the recording media dictates that the diffraction efficiency of each page varies as the reciprocal square of the total number of pages stored in the volume [24]. Thus, most of the reading light is wasted as a waste-product, with only a small (diffracted) portion of the energy containing the desired information. The energy inefficiency is particularly problematic if predetection optical processing is to be used, since the weak optical signal imposes strict limitations on the types of processing that can be performed.

Our method of solution involves the nonlinear optical phenomenon of two-beam coupling where two coherent beams of light intersecting in a photorefractive crystal or similar nonlinear medium interact to exchange energy unidirectionally so that one beam (the signal beam in Fig. 2) gains energy as the other (the pump beam) loses energy [25]. By using two-wave mixing, a spatially modulated weak beam can be amplified at the expense of a coherent pump beam with high fidelity. Under appropriate conditions, almost all of the pump beam energy can be diverted into the useful optical signal beam. By using the otherwise wasted light (which carries no useful information) as the pump beam to amplify the weak information beam from the memory as shown in Fig. 3 for the 3D optical memory, the overall energy efficiency can be improved significantly. A similar technique can be used for the 2D case. Such an amplified memory retrieval technique will be crucial to further preprocess the data optically, as described in the following sections. A brief discussion of photorefractive two-wave mixing is given in the next section in which the key parameters relevant to this program are highlighted.

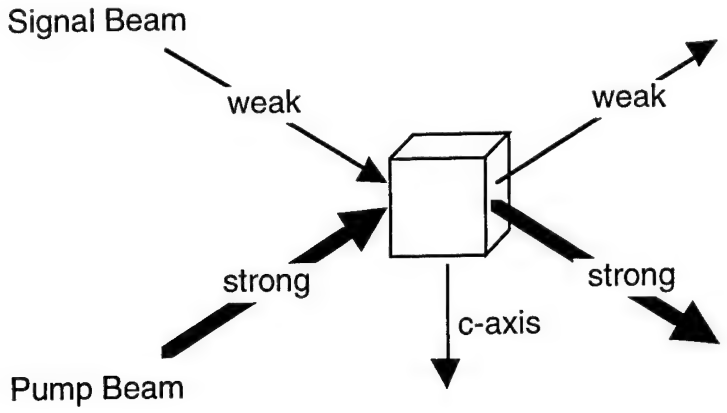

Fig. 2 Nonlinear Optical Two-Beam Coupling.

Nonreciprocal gain in one direction determined by crystal parameters

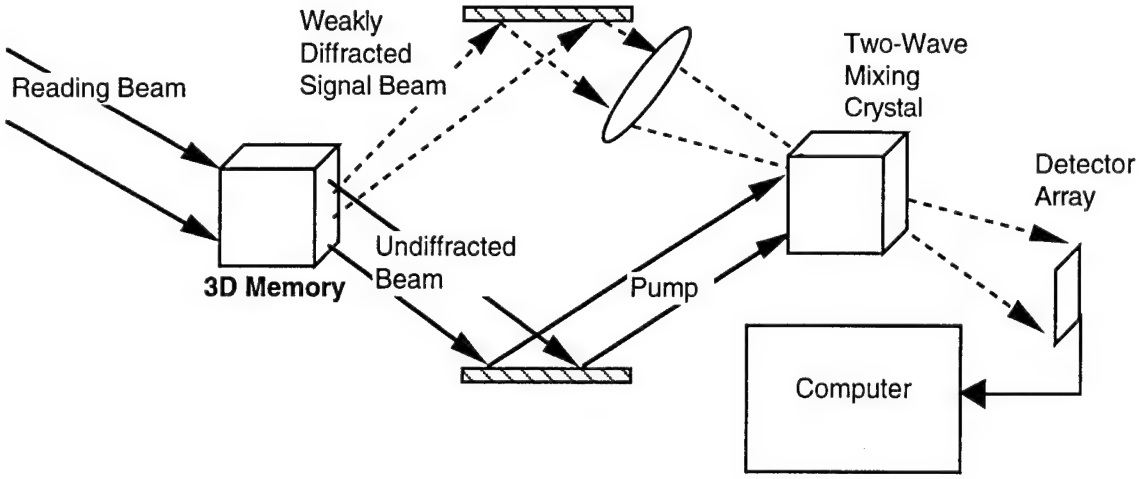

Fig. 3 Energy Efficient Extraction of Data from 3D Optical Memory.

2.2.2 Photorefractive Two Wave Mixing

Two-wave mixing, also known as two-beam coupling, is a process by which energy can be exchanged between two coherent beams of light in a photorefractive crystal. It can be thought of as a high gain, coherent amplifier. This occurs in photorefractive crystals where the dynamic index grating is 90 degrees out of phase with the intensity grating that produces it. In such a case, the diffraction of light is built up preferentially in one direction, and the intensity of one beam increases as the other depletes. The process was illustrated schematically in Fig. 2. The energy exchange is very efficient (limited by absorption in the crystal) and there is no phase cross talk between the two beams. In crystals such as SBN and $BaTiO_3$, high coupling gain occurs naturally due to their large electro-optic coefficients. In crystals with smaller electro-optic coefficients such as GaAs and BSO, however, large coupling gains can be achieved only if high external electric fields are applied to the material [26] in conjunction with a slight frequency shift between the two interacting beams.

One of the most important parameters that governs the overall speed performance of memory systems that incorporate photorefractive two-beam coupling is the speed of the photorefractive response. To maintain a high data transfer rate, the photorefractor must not impede the memory system with a response rate that is too slow (e.g., conventional $BaTiO_3$ crystals that respond on second time scales at $1W/cm^2$ intensities are too slow).

We have performed some system analysis to more accurately estimate the speed requirements for using photorefractive two-wave mixing for parallel access optical memory. In the simplest scenario where a weak signal that cannot be readily detected must first be amplified, the following simple

argument is given as an example of the analysis. If each binary data page that is read out in one step holds 1000×1000 bits, which is roughly 10^5 bytes of data, and we wish to maintain at least 100 Mbyte/sec data transfer rate in going from the long-term storage medium (volume hologram or disk) to the detector array/RAM (random access memory), the photorefractive amplifier must respond in no more than 1 msec. This immediately rules out any conventional ferroelectric crystal (such as $BaTiO_3$ from traditional sources), since their nominal time constants are on the order of 1 sec at 1 W/cm^2. Left to consider are either the new, fast ferroelectric crystals (Rockwell or MIT) or semiconductor or sillenite crystals. The ferroelectric crystal option is desirable because of their large dynamic range and hence strong coupling.

2.2.3 Fanning Noise in Two Beam Coupling

One key technical problem in a photorefractive optical amplifier is that imposed by photorefractive stimulated scattering, also known as "fanning." Fanning is scattered noise that occurs spontaneously but is amplified within the photorefractive crystal as the scattered waves propagate through the crystal. Not only does it compete for photorefractive gain with the signal beam, but it can also significantly degrade the fidelity of the amplified signal beam upon exiting from the crystal. Previous studies performed by personnel from the Applied Optics and Optical Information Processing departments indicate that fanning will almost always occur when the gain-thickness product exceeds a certain threshold (depends on crystal). Since high-gain amplifiers are required, an effective technique to either suppress or control fanning is required. Mechanical methods to suppress fanning have been proposed and demonstrated with some degree of success; but for packaging reasons and deployment considerations, nonmechanical solutions are sought. One important observation that we have made is that the inherent photorefractive time constant and the time required for the onset of fanning differ greatly. In all cases, more time is required for strong fanning to be established than for photorefractive two-beam coupling. Progress in theoretical modeling and experimental verification of the fanning process in photorefractive two-beam coupling are discussed in Section 3.4.

2.3 Optical Image Switching/Routing System

In a volume holographic memory system, the reconstructed output is originally in a two-dimensional (page) format in the optical domain. Before it is detected and converted into an electronic data pattern, the output can be optically processed in parallel to increase the functionality of the memory system to rapidly provide higher level functions such as sorting. We have demonstrated one such function; namely, the rapid shuffling of data blocks in arbitrary order,

using a unique approach illustrated in Fig. 4 [27]. In the example illustrated in the figure, a page of data is divided into N horizontal blocks. A set of phase gratings is aligned with the blocks, each with a unique spatial frequency so that a Fourier transform lens focuses the light from each block to a unique horizontal location at the back focal plane. A multichannel acoustooptic deflector is placed at the back plane, with each vertically oriented channel aligned with each focused block. The light in each channel is deflected vertically in proportion to the drive frequency used to energize the acoustic wave in the channel. Another Fourier transform lens then translates the variable vertical angle deflection into a vertical spatial shift, yielding a page in which the blocks have been rearranged vertically and arbitrarily. The processed or sorted data using such means can then be detected and converted into an already processed electronic output, relieving the user from performing such time-consuming operations. Our progress and accomplishment in this area are given in Section 3.5.

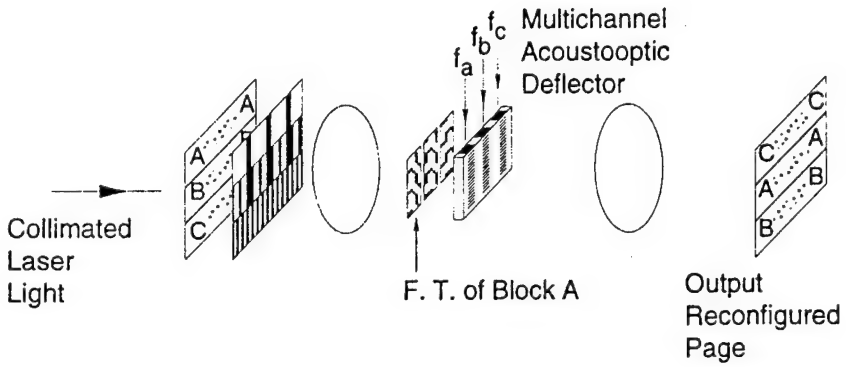

Fig. 4 Optical Data Block Shuffling System (the input set of data blocks can be arbitrarily re-ordered or shuffled in parallel).

3.0 Progress

3.1 Volume Holographic Content Addressable Memory (CAM) System Demonstration

During the course of this program, we have finished setting up a bench-top, content addressable memory demonstration system. The experimental configuration is illustrated schematically in Fig. 5. A laser beam (488nm) from an argon laser is split into a reference beam and an object beam by a variable beam splitter consisting of a half-wave plate ($\lambda/2$) and a polarizing beam splitter cube (PBS). Both beams are spatially filtered and collimated by SF1-L1 and SF2-L2, respectively. The reference beam is directed to a lithium niobate crystal (10mm $\times$ 10mm $\times$ 10mm) via a motorized two-dimensional scanning mirror (2DSM) whose orientation is controlled by a personal computer. A polarizer P2 is used to filter out the undesirable polarization component (in the plane of the drawing) of the reference beam. A lens L2 images the plane of the scanning mirror to the center of the lithium niobate crystal (LNB) crystal so that each mirror orientation corresponds to a specific value of the wave-vector (**K**) of the reference beam. Lens L5 focused the reference beam on the plane of a CCD camera (CCD1), which is monitored by the TV monitor (TV1). In the object arm, a two-dimensional pattern can be selected from a library of pictures (e.g., hundreds of fingerprints and photos of faces of people, all of which have been digitized and stored in an electronic memory) and displayed on a liquid crystal television (LCTV) to encode the picture on the object beam. Lenses L4 and L6 relay the plane of the LCTV (with appropriate demagnification) to a second CCD camera (CCD2) that is monitored by TV2. The LNB crystal is placed between L4 and L6 in the proximity of the back focal plane of lens L4

To record a set of pictures holographically in the LNB crystal by angular multiplexing technique, each picture is sequentially displayed on the LCTV, and the spatially modulated object beam is allowed to interfere inside the LNB crystal with the reference beam, which is characterized by a unique value of wave-vector **K** (dictated by the orientation of 2DSM) associated with each input picture. This specific value of **K** represents the address of the corresponding picture. The exposure time is managed by shutters (SH1 and SH2), which are controlled by the personal computer. Different exposure schemes can be preprogrammed and fine-tuned to improve the uniformity of the diffraction efficiency of all the holograms.

When the recording process is complete, any one of the recorded pictures can be retrieved from the volume holographic storage by sending the corresponding address to the 2DSM so that the

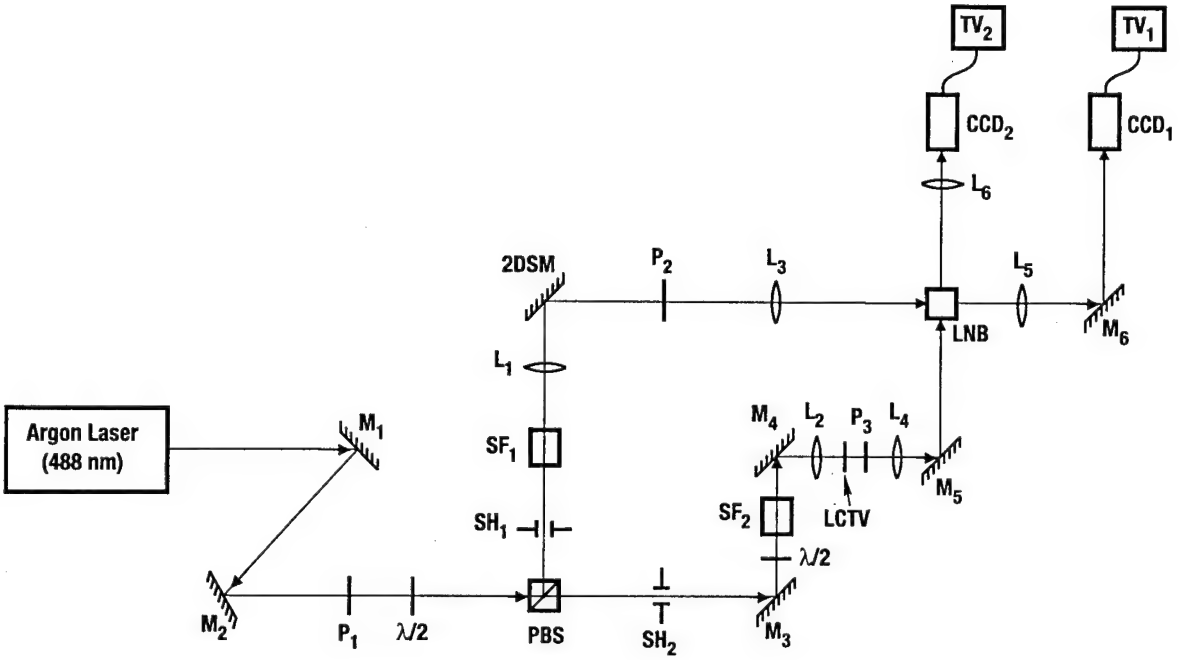

Fig. 5 Experimental Configuration.

multiplexed holograms are read out by the reference beam with the appropriate **K**-vector. The retrieved picture is imaged on CCD2 and displayed on TV2. This mode of operation allows parallel access to any one of the stored pictures. In other words, it is a parallel access page-oriented holographic memory system. The potential advantages of such a system include large storage capacity (> 1 GByte/cm^3), fast access time (~ submillisecond, using acoustooptic beam scanner), and high data transfer rate (~ 100 MByte/sec, limited by the readout electronics).

The same system can also be used as an optical pattern recognition system or a content addressable memory system. Instead of illuminating the multiplexed volume holograms with the reference beam, it can be illuminated with the object beam encoded with any spatial information displayed on the LCTV. The diffracted output (or readout) from the holograms then displays on CCD1 and TV1 the cross-correlation of the input pattern with all the stored patterns. Depending on the input pattern, one of the following two cases can be distinguished. (1) When the input pattern is identical to either the whole or a part of one of the stored patterns, the corresponding correlation peak will be much stronger then the rest. The position of this strongest peak at the CCD can be detected and translated into a control signal which is used to tune the 2DSM to the specific orientation (representing the address of the best-matched pattern). The best-matched pattern is retrieved as the

LNB crystal is illuminated by this properly oriented (i.e., Bragg-matched) reference beam. This mode of operation can thus be used for pattern recognition as well as content addressable memory. (2) When the input pattern does not resemble any of the stored patterns, the intensity of the cross-correlation points will vary within a certain range (depending on the degree of mismatch). A decision can be made based on the strength of the strongest correlation peak (or peaks) relative to the rest to either interprete the result as "no qualified match" or to recall the corresponding pattern(s) for further inspection by other means.

Using the configuration illustrated in Fig. 5, we have successfully demonstrated the basic operations of storage, recall, and correlation using 1000 finger prints. Quantitative characterization of the system performance requires further studies. Performance parameters such as the signal-to-crosstalk ratio, the diffraction efficiency and uniformity (in diffraction efficiency) of the holograms have yet to be determined; and technical issues such as the precision and repeatability of the mirror position controller need to be addressed.

3.2 Sensitivity Measurement of Photorefractive Two-Beam Coupling

An experimental investigation has been carried out to study the practical limit on the minimum input image intensity required in a photorefractive amplifier [28–30]. The understanding of this practical limit is very important, because the intensity of the optical image obtained from a volume holographic parallel access memory is expected to be very weak due to the low diffraction efficiency of the multiplexed holograms [9, 10, 12, 31–33]. Using an argon ion laser (514.5nm), a barium titanate crystal, and a pair of optical power meters with silicon detectors (Model 1835-C Multi-Function Optical Meter, from Newport Corporation), we have successfully demonstrated the amplification for an extremely weak binary image (with a total power of about 0.1nW) and the detection of a selected pixel (carrying an optical power of a few pW) within that image. We also compared the temporal development of the contrast ratio of the amplified image (due to beam fanning effect [34, 35]) in two different barium titanate samples, one of which exhibits a relatively weak (and the other relatively strong) degree of beam fanning.

The experimental configuration is illustrated schematically in Fig. 6. A linear array of rectangular slits was illuminated by a collimated laser beam from an argon ion laser (514.5nm) and imaged onto two output image planes (using a two-lens imaging system followed by a 50/50 beam splitter) where the optical power average over an area of about $1mm^2$ was sampled by two detectors D1 and D2, centered at a bright region and a dark region, respectively. A photorefractive barium titanate crystal was placed between the two lenses in the path of the image carrying beam and oriented such

that it can efficiently transfer optical energy from a pumping beam (from the same laser) to the image bearing beam (designated the signal beam hereafter). By reducing the optical intensity of the signal beam (using a set of neutral density filters in conjunction with a pair of cross-polarizers) and monitoring the output of detectors D1 and D2 with and without the pumping beam, the contrast ratio of the output binary image (with and without the aid of a photorefractive amplifier) was measured as a function of the signal beam power (measured at the entrance face of the crystal).

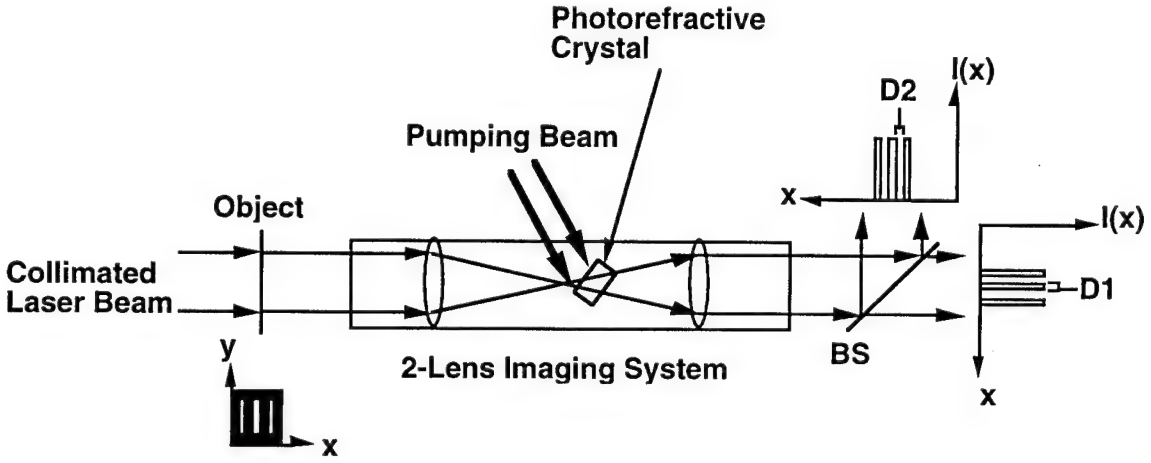

Fig. 6 A schematic illustration of the experimental configuration.

A typical experimental result is shown in Fig. 7(a) for the case when the pumping beam is turned off (i.e., the photorefractive amplifier was inactive) and when the optical power of the illuminating beam is varied continuously between 10pW and 10nW. While the output of Detector D1 (the detector monitoring the bright region) oscillated accordingly between maximum and minimum values, the corresponding essentially zero output from D2 revealed that the optical intensity in the dark region was below the detector sensitivity. At the minima, the reading from both power meters (in the most sensitive scale), fluctuated randomly somewhere between +10pW and -10pW, and apparently no distinction could be made between the bright and the dark regions. An oscillogram of these dark-current limited outputs is shown in Fig. 7(b). By turning on a 25mW pumping beam to activate the photorefractive amplifier, we were able to bring the signal level up above the dark current limit, distinguishing the weakly-illuminated region from the dark background.

A convenient way to illustrate the effect mentioned above is to leave the pumping beam on and monitor the output from the two detectors as the signal beam is switched on/off. The resulting oscillograms for different signal beam powers (i.e., a total input optical power of the signal beam of 10nW, 1nW, and 0.1nW, measured in front of the photorefractive crystal) are shown in

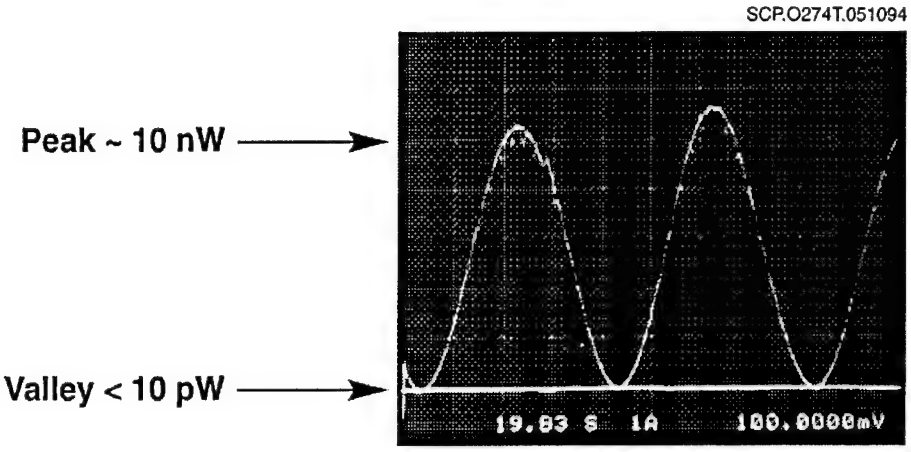

(a)

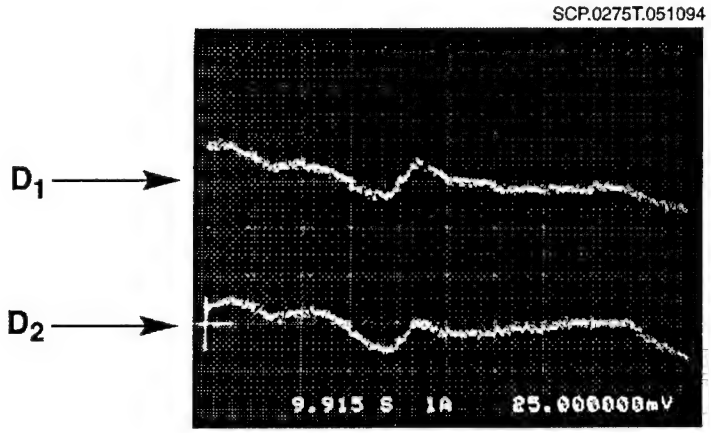

(b)

Fig. 7 Output from detectors D1 (upper trace) and D2 (lower trace) when the input optical power (a) varies from a few pW to about 10nW, (b) is fixed at a few pW.

Fig. 8(a), (b), and (c), respectively. The ON/OFF state of the input signal beam is indicated at the top and the bottom parts of the figures, and the reading from the power meters (optical power in nW) is given on the right. The difference in the reading from the two detectors (80nW vs 30nW) when the signal beam is off is due mainly to the deviation of the beam splitting ratio from 50/50 for the p-polarized beam. This can be balanced by using a variable beam splitter or an appropriate neutral density filter. Alternatively, the factor can also be normalized in determining the contrast ratio of the amplified image. The normalized contrast ratios [defined as (output of D1/output of D2) $\times$ (reflectance of beam splitter BS/transmittance of beam splitter BS)] corresponding to the three cases shown in Fig. 8(a), (b), and (c) are 3.75, 1.63, and 1.06, respectively. Note that in case (c),

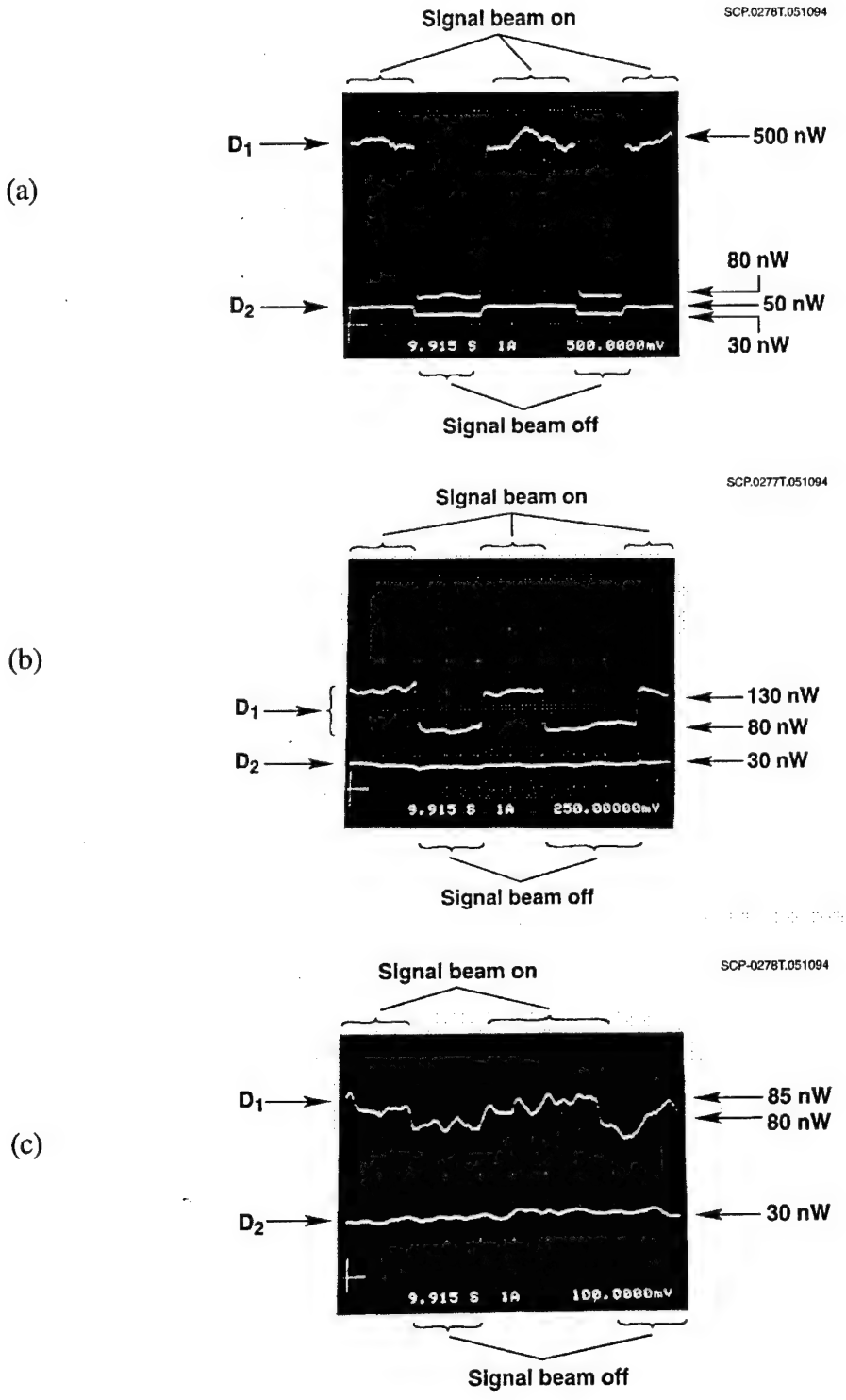

Fig. 8 Output from detectors D1 (upper trace) and D2 (lower trace) when the pumping beam is fixed (at 25 mW) and the signal beam is switched on/off. The total input power of the signal beam is (a) 10 nW; (b) 1 nW; (c) 0.1 nW.

the dark and the bright bars are barely discernible. Hence, we consider the minimum input signal power required for the particular photorefractive amplifier to be approximately 0.1nW. At this input power level, the actual optical power impinging on detector D1 (equipped with a sampling aperture of about $1mm^2$), with the photorefractive crystal removed, is well below the sensitivity of the detection system. Under such condition of ultra-weak illumination, the signal will be buried in the dark current noise of the detection system without the aid of optical amplification.

To determine the factor that limits the minimum input power, we measured the stray light at various locations and found that even when the signal beam was switched off, the stray light level measured at the entrance face of the was about 0.4nW, about four times the signal power. We speculate that the sensitivity of our system was limited by the background stray light. A more thorough understanding of this limiting factor requires further investigation.

The experimental results described above certainly depend on the characteristics of the specific photorefractive crystals. Our results, however, are comparable to those obtained by using a similar technique in which a bismuth silicon oxide (BSO) crystal with an applied electric field was used as the optical amplifier [36]. In some crystals the sensitivity can be much lower due to the strong beam fanning effect. To illustrate this point, we monitored the temporal development of the amplified image for two different barium titanate crystals with significant differences in the degree of beam fanning effect. In these experiments, the signal beam was kept constant at 1nW, and the amplified signal was monitored as the pumping beam (~25mW) was switched ON. The experimental results are shown in Fig. 9 (a) for crystal with strong beam fanning and in 9 (b) for the case of weak fanning. In both cases, the contrast ratio (output of D1/output of D2) first increased as the pumping beam was turned on, and gradually degraded (due to beam fanning) to a lower steady state value. A substantial degradation was observed in Case (a).

In summary, we have used two-beam coupling in a photorefractive barium titanate crystal to demonstrate the detection of a binary image in a region where the optical power was on the order of a few pW, which is below the sensitivity (~10pW) of our silicon detector. The sensitivity limit was successfully overcome by using the photorefractive crystal as an optical preamplifier. For a given photorefractive amplifier (i.e., a given crystal and a specific experimental configuration), the contrast ratio of the amplified image depends on the input optical power. In the regime where the input image intensity is extremely weak, the contrast ratio of the amplified image decreases monotonically as the input image intensity is reduced. For the photorefractive amplifier under investigation, the contrast ratio of the amplified image approaches 1, and the signal was no longer

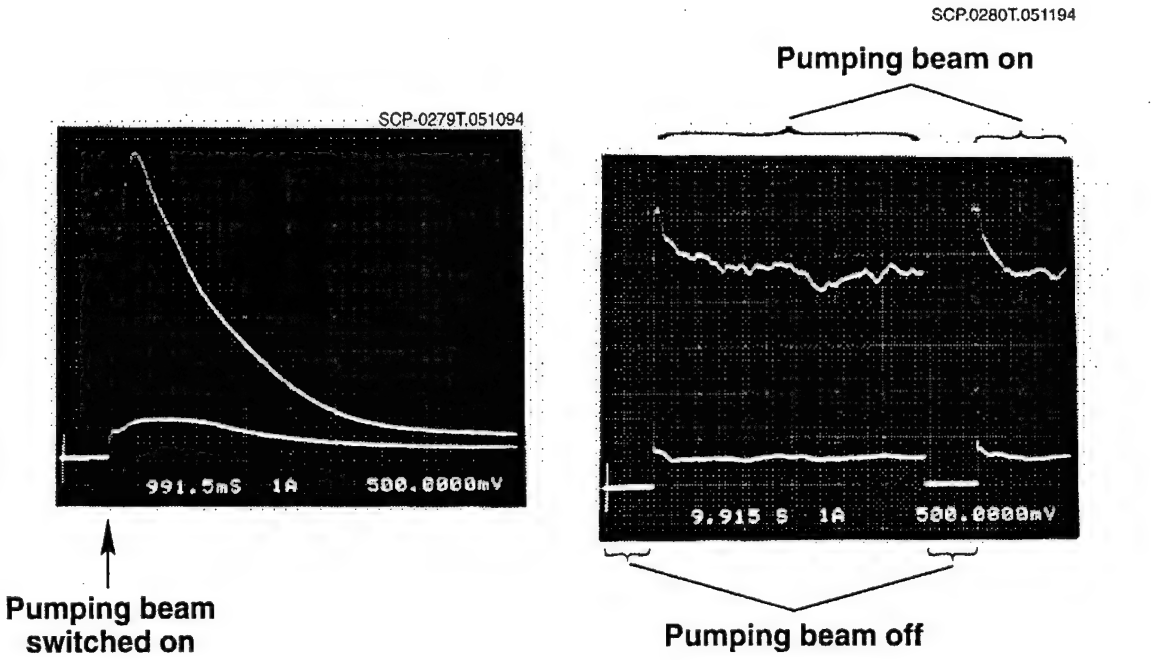

(a) (b)

Fig. 9 Output from detectors D1 (upper trace) and D2 (lower trace) when the signal beam is fixed (at 1 nW) and a pumping beam (of 25 mW) is turned on for a photorefractive barium titanate sample with (a) relatively strong beam fanning; (b) relatively weak beam fanning.

detectable when the total signal power was reduced to about a hundred pW or below. Although the numbers reported above do depend on the particular photorefractive crystal used and the specific experimental configuration, the results represent a useful example of the performance of a photorefractive amplifier and reveal that photorefractive amplifiers can be very useful under certain conditions.

3.3 High-Speed, High-Gain Photorefractive Amplifier Demonstration

3.3.1 Two-Beam Coupling in Fast SBN

We have performed some two-wave mixing experiments on the thin SBN sample acquired from the ferroelectric crystal growth department within the Science Center. The crystal is less than 1 mm thick and would not be suitable for actual use as an amplifier, since the overall gain would be too low. Nevertheless, we can measure the coupling constant, which is a measure of the exponential gain per unit length, to determine whether the composition of the crystal is suitable for our

application. Our experiments indicate that a maximum net gain constant of 17 cm^{-1} is possible at a response time of 15 msec (at 1 W/cm^2 intensity). With such an exponential gain coefficient, amplification factors exceeding 3,000 should be possible with a 5 mm thickness. Although the speed is not as fast as what we desire, the figure that we measured for the response time is at least 2 orders of magnitude faster than the other SBN and $BaTiO_3$ crystals in our laboratory. We have thus far been unable to procure a SBN crystal that is faster and thicker (for larger beam coupling) than the thin plate that was evaluated earlier in the course of this program (reported in bimonthly report # 3).

3.3.2 Fast Two-Beam Coupling in Barium Titanate Crystal

At the beginning of this program, we performed some system analysis to more accurately estimate the speed requirements for using photorefractive two-wave mixing for parallel access optical memory. The relevant performance parameters are i) the amplification factor that must be supplied to overcome large optical losses in both the retrieval and processing of data and ii) the speed of the amplifier which limits data throughput of the system. We have concentrated our efforts on the holographic storage system, although disk-based parallel access memories work with similar parameters. In holographic storage systems, multiple pages of data are superimposed in the same storage volume by writing each hologram with some unique characteristic such as the wavelength of recording [37], angular orientation of the reference beam [38] or reference beams, each with a unique spatial phase modulation [39]. The multiplexed storage results in a high density storage format with extremely high speed access characteristics. These benefits come at the price, however, of reduced energy efficiency in the read process, since very little of the optical power that is used to interrogate the memory is converted into an output data modulated beam. Typically, the diffraction efficiency of each holographically recorded data page is not larger than 10^{-6} [24]; which means that if the memory is interrogated with a beam with an optical intensity of 1 W/cm^2, the actual output beam with the retrieved data has an intensity of 1 $\mu W/cm^2$.

The inherently low optical efficiency of holographic readout is compounded if optical processing is performed on the retrieved data in its optical form. If the insertion loss imposed by the optical processing performed on the output light is 20–30 dB, the overall optical insertion loss, including the diffraction efficiency of the hologram, ranges from 80 to 90 dB. The noise equivalent exposure density of very sensitive photodiode arrays is roughly $E \geq 0.2$ nJ/cm^2 [40]. If a total of 1 msec is allowed for detection, the noise equivalent intensity that the detector can reliably sense is $I \geq 0.2$ $\mu W/cm^2$. If a read beam intensity of 1 W/cm^2 is supplied to interrogate the crystal, an

insertion loss of 80 dB yields an output intensity of 10 nW/cm^2, which is several orders of magnitude below the detectable limit. An optical amplifier that is capable of preserving coherent spatial information is thus necessary to overcome such large insertion losses. To be most effective, such amplifiers should be placed just after the hologram to minimize the amplification of unnecessary noise.

An equally important parameter is the speed of the amplifier, which ultimately limits the volume of data that can be transferred from memory to the user per unit time. For example, if each page of data contains 1 million bits of data and the amplifier has a response time of 1 millisecond, the raw data throughput or transfer rate is 1 gigabit per second. Although our demonstrations are performed with smaller format pages (320 × 200), 1000 × 1000 bit pages are very realistic [41] with existing or developing spatial light modulator technologies. If the amplifier response time is increased to 10 milliseconds, the corresponding transfer rate becomes 100 megabits per second, which is almost two orders of magnitude higher than disk based systems.

Our technical goals for this portion of the project are twofold: i) achieve high gain photorefractive amplification (>1000x) with low scatter noise, ii) achieve fast response at reasonable intensities (1 millisecond @ 1 - 10 W/cm^2). The two goals are, of course, to be accomplished in unison. After evaluating many candidate crystals in the sillenite and ferroelectric varieties, a $BaTiO_3$ sample obtained from MIT [42] was identified as the most promising in providing the right balance of gain and speed. Indeed, this crystal seemed to be one of the most sensitive $BaTiO_3$ crystals that we have seen in our laboratory.

As a comparative demonstration, we performed video image amplification of an object beam that carries video via a liquid crystal television using the MIT $BaTiO_3$ crystal compared against the same using a "standard" $BaTiO_3$ crystal from Sanders. The experimental setup is shown in Fig. 10, in which the probe (to be amplified) is a very weak beam spatially modulated with a liquid crystal display (320 × 200 pixels, video frame rate = 30 frames/sec). The probe is imaged through the photorefractive crystal onto an output television camera. A strong pump beam (more than 10,000 times higher in intensity than the probe) is derived from the same laser and is directed onto the photorefractive crystal at an optimum angle from the probe. Since the probe beam consists of multiple diffraction orders from the LCD, which interfere at the output to give rise to a "grid" pattern, the pump was focused to amplify only the center order to effectively suppress the output grid pattern. This is known as spatial amplification [43].

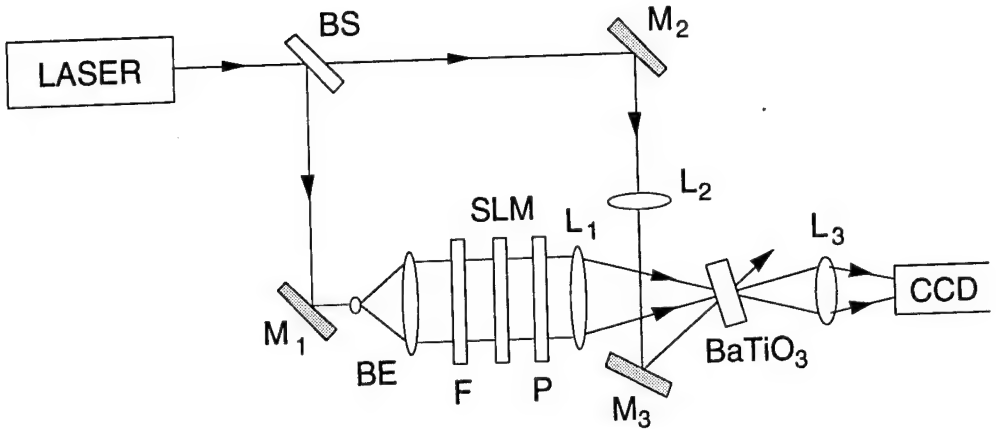

Fig. 10 Video Amplifier Experiment.

The videotape that is a part of this report shows the video animation sequence that is amplified by the MIT crystal. The important feature to note is the clarity of the frame-to-frame video transitions, which imply that the amplifier response is sufficiently fast to keep up with the video frame rate (33 msec). In comparison, the amplified video sequence performed by the Sanders crystal shows significant blurring between the frames with much of the fast "action" sequences completely suppressed. Only the stationary objects are amplified effectively, implying that the response of the Sanders crystal is too slow for video. The temporal response of the MIT crystal is illustrated in the oscilloscope trace shown in Fig. 11, which depicts the output probe beam when the input probe is suddenly turned on. Preliminary experiments showed that optical gains exceeding 300 is easily achievable at time constants of less than 18 msec, which is sufficient for video rates processing (at nominal optical intensities of the order of 1 W/cm^2). Further work is needed to achieve higher gain and higher speed with this crystal, which should be possible by judicious choice of beam focal parameters and crystal orientation.

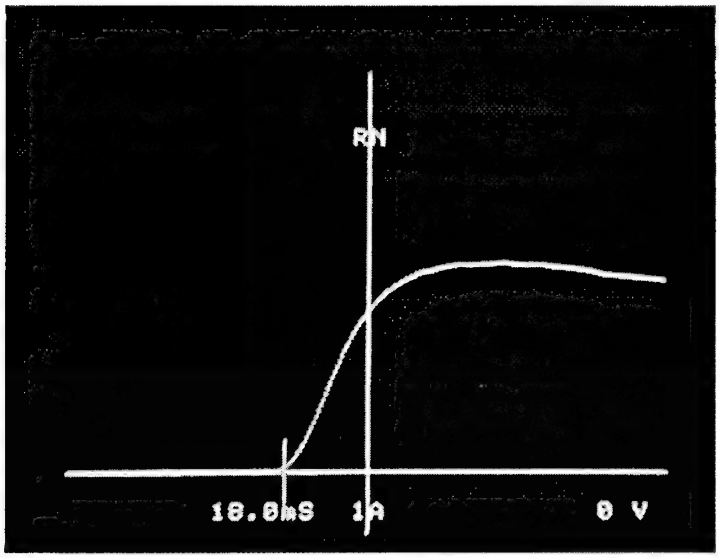

Fig. 11 Temporal Response of Two Beam Coupling in Fast $BaTiO_3$.

3.4 Theory and Experiment on Fanning Noise in Photorefractive Amplifier

The amplification of scattered light resulting in beam fanning is the primary source of noise in photorefractive amplifiers. Effective strategies for reducing beam fanning are thus critical in the development of useful photorefractive amplifier stages in any optical data processing system. While several such strategies have been developed, their use has been based largely on empirical observations of fanning behavior rather than a thorough understanding of the underlying physical processes. As a result, optimization of these fanning reduction techniques over a broad range of practically encountered conditions remains difficult. To develop the understanding necessary to optimize the noise behavior of photorefractive amplifiers, we have thus undertaken a detailed theoretical and experimental study of fanning dynamics.

The most effective techniques for fanning reduction have been based on the observation that the time required for the fanning beam to form in a photorefractive amplifier is usually several times the response time for optical signal amplification. Thus if the optical amplitudes incident on the crystal are varied on a time scale within the bandwidth of signal amplification yet are shorter than that required for the formation of the fan (often simply by moving the amplifying medium with the proper speed and orientation), fanning will be suppressed without deleterious effects on the amplified signal. This technique is only effective, however, when the fanning response time and the signal response time are well separated. If the two are comparable, either insufficient fanning

suppression or significant reductions in amplifier gain result. Since in most photorefractive materials of practical interest the observed fanning time is only 2–5 times the amplifier response time, clearly small variations in the fanning response time will significantly affect the efficacy of the technique of fanning suppression. Our study of the dynamics of the photorefractive fanning process described herein is thus motivated by the need to control the temporal response of this effect.

3.4.1 Physical Model

Of the several theories of photorefractive beam fanning, the most accurate descriptions are obtained when fanning is described as the result of the photorefractive amplification of scattered light. Since both amplification and scattering can be modeled fanning, which incorporates both effects should also be amenable to modeling. Unfortunately, the description of beam propagation and nonlinear interaction within a photorefractive crystal grows in complexity very quickly when multiple beams are introduced. While two beam models of photorefractive beam coupling are sufficiently detailed yet simple enough to give accurate analytic descriptions of the dynamics of beam amplification in the absence of fanning, complete inclusion of the effects of scattering require a many-beam coupling analysis that can be quite computationally intensive and not at all likely to provide closed form analytic results.

Our approach to this problem is to model the effects of scattering by introducing a small set of "auxiliary" beams into the standard two-beam coupling analysis. By controlling the parameters describing these auxiliary beams, we can account for much of the energy transfer and beam dispersal resulting from true scattering, yet do so in a manner more conducive to analytic coupled wave treatments. The use of this formalism is suggested by the fact that the fanned light in photorefractive amplifiers tends to aggregate into relatively localized beams rather than a uniform spray of scattered light. Thus we may hope that by using relatively few auxiliary beams we will achieve an accurate model of the physical processes at work in fanning. This can be thought of as an extension of previous work in which researchers modeled the photorefractive fan as a single plane wave. While such an approximation is too simplistic to describe the dynamic properties of beam fanning, the inclusion of additional auxiliary beams improves the results significantly.

In practice we find that much of both the static and dynamic behavior of photorefractive fanning can be achieved with the use of only two auxiliary beams to represent the amplified scattering process. Specifically, we model the fanning process as described in Fig. 12, in which a single optical pump beam is incident on a photorefractive material and scatters from imperfections both at

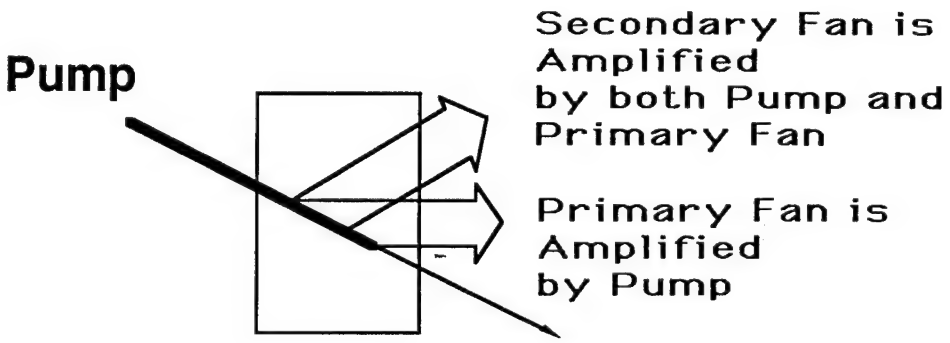

Fig. 12 Multiple Fan Beam Model.

the surface and in the bulk of the medium into a second beam, denoted the primary fan. This beam receives energy from the pump beam and is thus photorefractively amplified as it passes through the medium. At the same time, however, this primary fan beam is itself scattered into a secondary fan beam, which is also amplified photorefractively. This division of the fan beam into two components possesses a critical distinction from the single fan beam model used in earlier analyses. Specifically, we find that each step of beam amplification has a response time determined by the material and environmental parameters characterizing the photorefractive amplifier. Thus if the fanning process is treated as a single step of amplified scattering, it will have a response time equivalent to that of any amplified signal beam. Thus, any single fan beam model will fail to show the very disparity in response time that is maximized in the fanning suppression techniques we have described. Conversely, by breaking the fan process into multiple steps, we find that the secondary fan beam can have a formation time substantially longer than amplifier response time, the key experimental observation we are trying to describe. With this motivation we can now describe the two-component fan model, its predictions and their experimental confirmation in more detail.

If we model the fanning process as two steps of amplification and scattering as described above, the amplitudes of the coupled beams in the photorefractive material can be described according to the system of nonlinear equations:

Pump: $$\frac{dR}{dz} = \frac{i}{2}\Gamma_1 E_1 S$$

Primary Fan: $$\frac{dS}{dz} = \frac{i}{2}\left(\Gamma_1^* E_1^* R + \Gamma_2 E_2 Q\right)$$

Secondary Fan: $$\frac{dQ}{dz} = \frac{i}{2}\Gamma_2 E_2 S$$

Coupling Fields: $$\frac{dE_1}{dt} + \frac{E_1}{\tau} = \frac{R S^*}{\tau} \qquad \frac{dE_2}{dt} + \frac{E_2}{\tau} = \frac{S Q^*}{\tau}$$

where R(z,t), S(z,t) and Q(z,t) are the optical amplitudes of the pump, primary and secondary fanning beam, respectively; E_1 and E_2 are components of the space charge field within the medium; Γ_1 and Γ_2 are the photorefractive gain associated with the primary and secondary fan beams, respectively; and τ is the photorefractive response time. While this system of equations is vastly simpler than that describing the complete processes of amplification and scattering in a photorefractive medium, it is sufficiently complex that a full analytic solution remains unavailable. Nevertheless, it is sufficiently simple that numerical solutions may be achieved with minimal computational effort, and a variety of approximate analytic results can still be obtained. Furthermore, we shall show that these results describe sufficiently many of the effects we observe in experimental studies of fanning to validate our model.

While as noted earlier, exact analytic solutions to the full coupled system have not been obtained, some analytic results are available. In particular, we may obtain limiting results in the case of minimal beam depletion. Under this assumption the pump beam remains temporally constant as the primary fan beam (or equivalently the amplified signal beam) grows, and the secondary fan beam is assumed to be negligible during this amplification process. Once the primary fan approximately reaches steady state, it is then assumed constant and pumps the secondary fan. While this complete separation is somewhat artificial, exact numerical solutions of the coupled system show very little growth of the secondary fan before the primary fan grows large. Thus, even this rather primitive approximation reflects observed behavior with reasonable accuracy. The benefit gained from this approximation is an analytic expression for the turn-on time of the secondary fan beam in the undepleted limit.

Specifically, we have shown that each step of photorefractive amplification is associated with a response time of roughly $\Gamma L\tau/2$, where Γ is the gain associated with the amplification process and τ the photorefractive response time in the weak amplification limit. Thus, not only does the amplification time increase with increasing gain, but the fanning time in the two-component fan model must also be at least twice the amplification time. Furthermore, both the amplification and fanning times should increase linearly with interaction length in the material. These predictions are now easily tested by comparison with numerical and experimental results.

When we solve this system numerically for the interacting beam amplitudes using typical photorefractive parameters, we obtain solutions such as those shown in Fig. 13 below. Here, assuming a constant (undepleted) pumping beam, we see that the secondary fan does indeed grow with a characteristic response time larger than that of the amplified signal, but in this case the ratio of response times is closer to three than the predicted factor of two. This discrepancy may be explained by noting that the fan beam only reaches its maximum level through significant depletion of the amplified signal. Thus our limiting case solution, assuming the primary fan effectively ceases to grow after a single amplifier response time, will underestimate the actual fanning time.

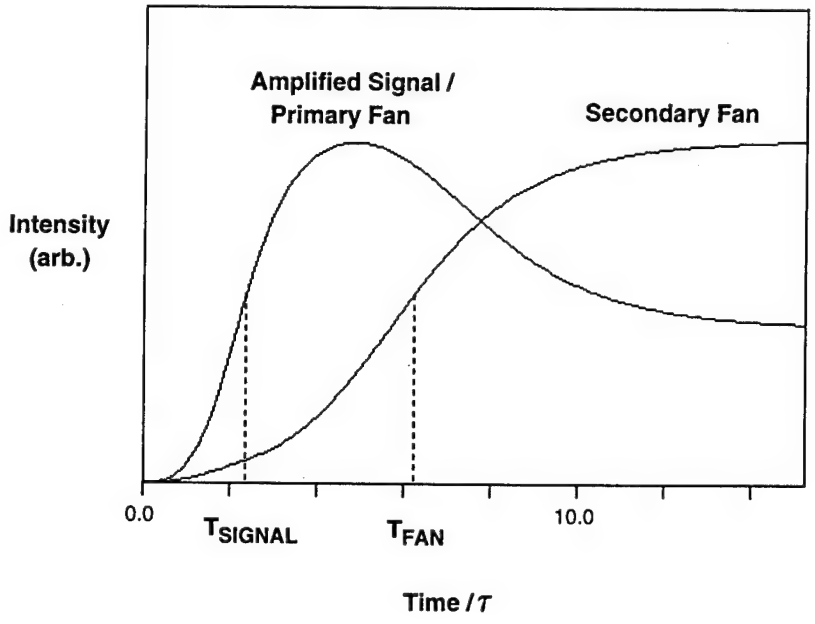

Fig. 13 Numerical Solutions to Growth of Signal/Primary Fan and Secondary Fanning Gratings.

In addition to this dynamic behavior, our two-component fan model describes other observable fanning phenomena that are not considered in earlier models. In particular, since the

different fan components exit the photorefractive material at different angles, our model provides a description of the temporal evolution of the spatial structure of the fan beam, which may also be tested to assess the model's validity.

3.4.2 Experimental Verification of Theoretical Model

Two main predictions result from our model. First, we predict that the fanning response time will be roughly twice the amplifier response time; and that both response times will increase linearly with crystal thickness. Second, this two-part growth indicates that the spatial distribution of fanned light should shift to greater angles during the fan formation process as first the primary and then the secondary fan dominates.

The first of these predictions is tested by observing two-beam coupling in a wedge-shaped sample of $BaTiO_3$. By varying the position of incidence of the input beams along one face of the crystal as shown in Fig. 14, the interaction length can be varied continuously from less than 0.5 mm to several mm. In each case the intensities of the amplified signal beam transmitted through the crystal and the fanning beam that formed were recorded on an oscilloscope and stored. A sample trace of these beams is reproduced in Fig. 15 and, while the agreement is not exact, upon comparison with Fig. 13 shows features of differential response time and signal beam depletion very similar to those present in the theoretical result.

By deriving response times from data such as that given in Fig. 15 for a variety of interaction lengths, the dependence of amplifier and fanning response time on interaction length was determined. This data is plotted in Fig. 16 for interaction lengths ranging from 0.5 to 4.0 mm in the wedged sample, with triangles and circles representing the amplifier and fanning response times, respectively. We see that as predicted, both response times appear to grow linearly with the interaction length L; and furthermore, that the slope of the fanning time data is indeed roughly twice that of the amplification time data, as we had predicted from our analytic approximation to the coupled system. The predicted linear behavior of the fanning time breaks down, however, for sufficiently large interaction lengths. We believe this deviation from the predicted linear behavior is an artifact of the peculiar geometry of our wedge-shaped sample. At interaction lengths greater than 2 mm, light from the fanning beam can reach the corner of our sample and internally reflect, allowing other nonlinear optical wave mixing effects to occur and compete with the amplification and fanning processes. Such effects, however, are not intrinsically related to the fanning process and can usually be removed in practice by suitable choice of experimental geometry.

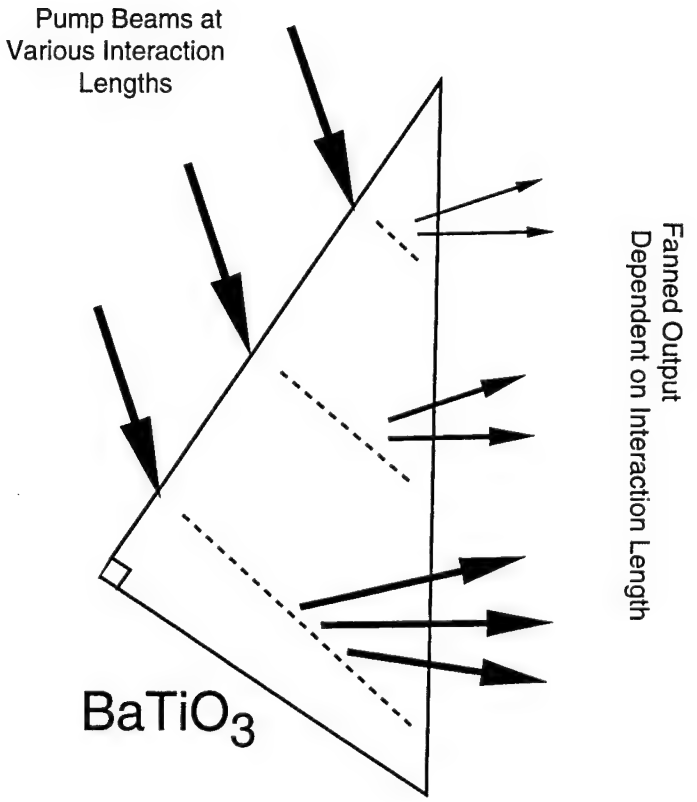

Fig. 14 Wedge-shaped Sample of $BaTiO_3$.

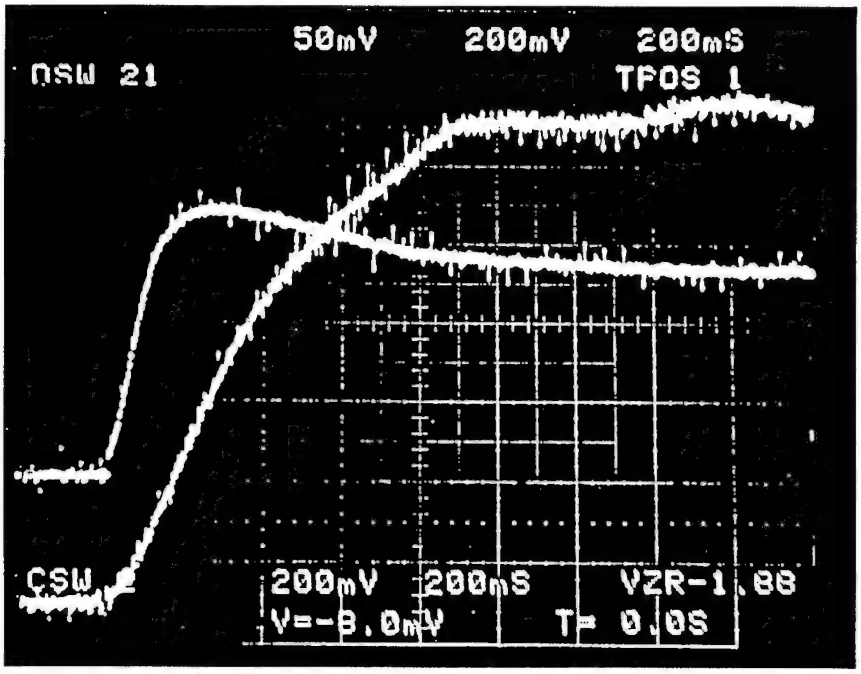

Fig. 15 Fan and Signal Temporal Response.

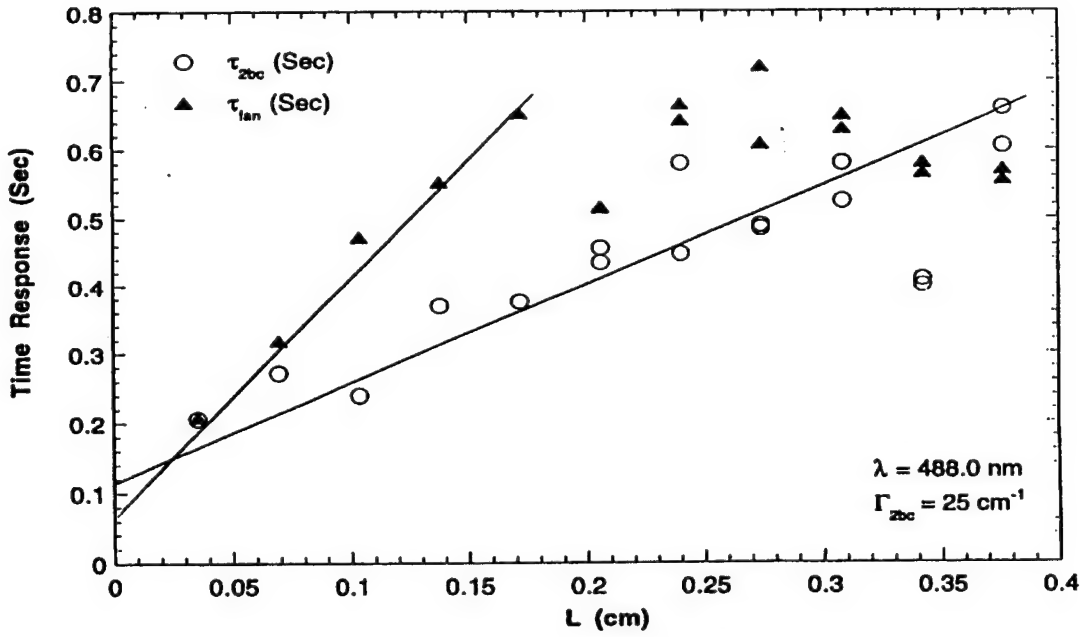

Fig. 16 Two-Beam Coupling and Fanning Response in Wedged $BaTiO_3$.

In addition to our examination of the response time of the fanned light, we investigated the spatial distribution of the fan. While the most complete test of our model would involve a detailed measurement of the temporal evolution of this spatial distribution and thus indicate whether several fan steps at different angles of propagation come into play as the fan develops, our wedge-shaped material allows us to determine much of the same information with a much simpler test. Specifically, while our model predicts that secondary fanning processes play an increasing role as the fan nears steady state, it also indicates that such processes predominate only when the amplifying material possesses sufficient gain to allow the primary fan beam to grow to a significant level and then deplete into the secondary fan. In cases of limited gain, only the first of these two processes would occur to any significant degree and thus the predicted deviation angle of the observed fan would be less. In contrast, previous theories of beam fanning by simple amplified scattering suggest that the spatial structure of the fan should be independent of gain. By observing the spatial distribution of light fanned from the wedge at different interaction lengths, we can see whether this distribution shows a shift or simply varies in overall intensity as the total amplifier gain (proportional to exp[ΓL]) is varied, and thus assess the validity of our multistep fan model.

When such a measurement is conducted and the fan beam is sampled by a linear diode array at various interaction lengths, a series of plots is generated (Fig. 17). Here measured fan beam intensity is plotted vs. scattering angle, with increasing scattering angle plotted to the right. We see

that while for small interaction lengths a maximum fan at relatively small angles is observed, when the interaction length is increased to several mm (and significant depletion into the fan occurs) the distribution of the fanned energy does indeed shift to larger scattering angles, as predicted in our model. Interestingly, once this larger angle fanning peak is reached, further increases in interaction length do not appear to cause a further shift in the fan distribution. This suggests that only two steps may indeed be sufficient to provide an accurate description of the full dynamics of the fanning process.

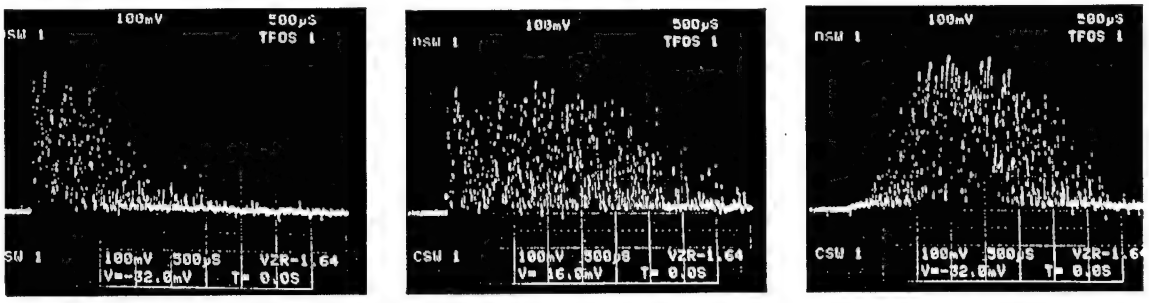

(a) (b) (c)

Fig. 17 Spatial Structure of Fan Noise Beam.

3.4.3 Conclusions for Fanning Theory and Experiments

Both the spatial and temporal measurements of fanning characteristics we have conducted tend to corroborate our multistep fanning model. Furthermore, the analytic results we have gleaned from this model, in particular the relationship between the response times for amplification and fanning, appear to be borne out both in numerical simulations and in practice. Nevertheless, several issues remain to be resolved. In particular, our simplified analysis indicates that fanning times should always be on the order of twice the signal amplification time; yet various experimental studies have shown ratios between these response times as high as five to one. While some of this discrepancy results from the effects of signal beam depletion as described earlier in this report, the explicit relationship of this ratio to the physical characteristics of the amplifier has yet to be determined. As this ratio most directly affects our ability to fanning effects via temporal dithering without adversely affecting amplifier gain, further analysis of our model and possibly modifications thereof may be appropriate. In addition, we have yet to directly measure the temporal evolution of the spatial structure of the fan beam. While our interaction length measurements suggest our model is accurate, a thorough examination of the spatial and temporal properties of the fan beam will allow this determination to be made with greater confidence.

3.5 Reconfigurable Optical Image Switching/Routing System Demonstration

Details of our progress and accomplishment in this area has been published [27]. A reprint of the paper is included in Appendix A1.

4.0 References

1. E.N. Leith, A. Kozma, J. Upatneiks, J. Marks, N. Massey, *Appl. Opt.* **5**, p. 1303 (1966).

2. J.P. VanHeerden, *Appl. Opt.* **2**, p. 393 (1963).

3. E. G. Ramberg, *RCA Review* **33**, p. 53 (1972).

4. L. d'Auria, J.P. Huignard, C. Slezak, E. Spitz, *Appl. Opt.* **13**, p. 808 (1974).

5. J.J. Amodei, D.L. Staebler, *Appl. Phys. Lett.* **16**, p. 605 (1971).

6. H. Fleisher, P. Pengelly, J. Reynolds, R. Schools, G. Sincerbox, "An optically accessed memory using the Lippmann process for information storage", from *Optical and Electrooptical Information Processing,* J.T. Tippett et al., eds., pp. 1–30, MIT Press, Cambridge (1965).

7. L. Hesselink, "Holographic information storage", CLEO, Anaheim, CA (1994).

8. M. Neifeld, M. MacDonald, *Opt. Lett.* **19**, p. 1483 (1994).

9. F.H. Mok, M.C. Tackitt, H.M. Stoll, *Opt. Lett.* **16**, p. 605 (1991).

10. F.H. Mok, *Opt. Lett.* **18**, p. 915 (1993).

11. G.W. Burr, F.H. Mok, D. Psaltis, "Storage of 10,000 holograms in $LiNbO_3$:Fe", CLEO, Anaheim, CA (1994).

12. S. Tao, D.R. Selviah, J.E. Midwinter, *Opt. Lett.* **18**, p. 912 (1993).

13. C. Gu, J. Hong, I. McMichael, R. Saxena, F.H. Mok, *J. Opt. Soc. Am. A* **9**, p. 1978 (1992).

14. K. Curtis, C. Gu, D. Psaltis, *Opt. Lett.* **18**, p. 1001 (1993).

15. K. Curtis, D. Psaltis, *J. Opt. Soc. Am. A* **10**, p. 2547 (1993).

16. M.C. Bashaw, B. Hesselink, *J. Opt. Soc. Am. B* **11**, p. 1820 (1994).

17. A. Yariv, *Opt. Lett.* **18**, p. 652 (1993).

18. J. H. Hong, P. Yeh, D. Psaltis, D. Brady, *Opt. Lett.* **15**, p. 344 (1990).

19. D. Psaltis, F. Mok, H.Y.S. Li, *Opt. Lett.* **19**, p. 210 (1994).

20. F. Micheron, G. Bismuth, *Appl. Phys. Lett.* **23**, p. 71 (1973).

21. Yong Qiao, S. Orlov, D. Psaltis, R.R. Neurgaonkar, *Opt. Lett.* **18**, p. 1004 (1993).

22. A. Kewitsch, M. Segev, A. Yariv, R.R. Neurgaonkar, *Opt. Lett.* **18**, p. 1262 (1993).

23. D. Psaltis, M.A. Neifeld, A. Yamamura, S. Kobayashi, *Appl. Opt.* **29**, p. 2038 (1990).

24. D. Psaltis, D. Brady, K. Wagner, *Appl. Opt.* **27**, p. 1752 (1988).

25. P. Yeh, A. Chiou, J. Hong, *Appl. Opt.* **27**, p. 2093 (1988).

26. J.P. Huignard, A. Marrakchi, *Opt. Lett.*, **6**, p. 622 (1981).

27. E.G. Paek, J.H. Hong, T.Y. Chang, and D. Pletcher, *Opt. Lett.*, **20**, p. 1904 (1995).

28. J. Joseph, P.K.C. Pillai, and K. Singh, *Appl. Opt.* **30**, p. 3315 (1991).

29. J. Hong, A. Chiou, and P. Yeh, *Appl. Opt.* **29**, p. 3026 (1990).

30. P. Yeh, et al., *Opt. Eng.* **28**, p. 328 (1989).

31. D.L. Staebler, W.J. Burke, W. Phillips, and J.J. Amodei, *Appl. Phys. Lett.* **26**, p. 182 (1975).

32. R.G. Zech, *Opt. and Photonics News* **3**, p. 16 (1992).

33. E.S. Maniloff and K.M. Johnson, *J. Appl. Phys.* **70**, p. 4702 (1991).

34. J. Feinberg, *J. Opt. Soc. Am.* **72**, p. 46 (1982).

35. W.S. Rabinovich, B.J. Feldman, and G.C. Gilbreath, *Opt. Lett.* **16**, p. 1147 (1991).

36. H. Rajbenbach, A. Delboulbe, and J.-P. Huignard, *Opt. Lett.* **16**, p. 1483 (1991).

37. W. J. Burke, P. Sheng, *J. Appl. Phys.* **48**, p. 681 (1977).

38. G.A. Rakuljic, V. Leyva, A. Yariv, *Opt. Lett.* **17**, p. 1471 (1992).

39. C. Denz, G. Pauliat, G. Roosen, T. Tschudi, *Opt. Commun.* **85**, p. 171 (1991).

40. EG&G array sensor data book

41. ARPA Broad Agency Announcement, "Holographic Data Storage Systems", ARPA Solicitation BAA 93-37 (Aug. 26, 1993).

42. MIT crystal obtained from the Crystal Physics Laboratory (Prof. C. Warde, Dr. M. Garret).

43. T.Y. Chang, J. Hong, *Opt. Lett.* **15**, p. 743 (1989).

5.0 Appendix

"Fast reconfigurable optical image switching/routing system", by E.G. Paek, J.H. Hong, T.Y. Chang, and D. Pletcher, *Opt. Lett.,* 20, p. 1904 (1995)

Fast reconfigurable optical image switching/routing system

Eung Gi Paek

National Institute of Standards and Technology, 255/A61, Gaithersburg, Maryland 20899

John H. Hong, Tallis Y. Chang, and David Pletcher

Rockwell Science Center, Thousand Oaks, California 91360

Received July 3, 1995

A novel system that is capable of switching/routing two-dimensional images in arbitrary configurations is described. The switching network can be reconfigured in a few microseconds with high light efficiency.

Figure 1(a) shows a typical point-to-point switching/routing network commonly used in telecommunications.[1] The signals that flow from input to output nodes are purely temporal, with the interconnection network characterized by the following requirements: arbitrary input/output interconnection, fast (within a few microseconds) reconfiguration, high light efficiency, and optical transparency that does not impose any intermediate speed bottlenecks owing to photon/electron conversion.

Our goal is to generalize the conventional point-to-point network to permit the routing of two-dimensional spatial information illustrated in Fig. 1(b), while satisfying the above requirements. This generalization may find a variety of new applications in future multimedia communications. It can also be used for the parallel manipulation of data retrieved from a volume holographic memory system, which can potentially yield large (e.g., 1024 × 1024) two-dimensional blocks of data in microsecond intervals.[2] Furthermore, it can be used to implement associative memories[3] or inference machines[4] when it is incorporated with a pattern-matching system.

Since the mid-1980's there have been substantial interest and activities in implementing the perfect shuffle algorithm[5] for digital optical computing and switching applications. The perfect shuffle uses multiple layers of shuffling interconnections interleaved with exchange/bypass switch arrays to achieve arbitrary configurations. Most implementations reported to date use arrays of prisms, lenses, or multiple holograms to provide the required magnification and interleave operations.[6–9] For a single-layer reconfigurable interconnection, rewritable holographic approaches that use photorefractive crystals might be considered.[10] However, in this case an additional fast beam steering device is required to provide the light path for the desired configuration in addition to the hologram recording process.

In this Letter we present a novel fast reconfigurable image crossbar/shuffling network that can be reconfigured within a few microseconds. Our approach is based on the following two simple concepts. First, with an acousto-optic beam deflector with a wide angular bandwidth, an image is spatially shifted in microsecond durations. Second, for efficient multiplexing a multichannel acousto-optic beam deflector (AOD) is used in conjunction with an array of phase gratings.

Figure 2 shows the principle of fast image shift by use of an AOD at the Fourier plane of a conventional coherent optical processor. In the system an input transparency is illuminated by a collimated monochromatic wave and is imaged at the output plane by a telescopic system that consists of two lenses, L_1 and L_2. If an AOD is inserted at the focal plane of lens L_1 and a rf signal with a variable temporal frequency is applied to it, the first-order diffracted image appears at the output plane displaced from the zeroth-order image. The amount of displacement of the first-order image is approximately proportional to the frequency of the rf signal for small displacements. Therefore one can shift an image freely by simply varying the frequency of the rf signal applied to the AOD. The shift can be achieved in a few microseconds, which is the time required for an acoustic signal to scan the Fourier spectrum of the input. The access time and resolution are basically limited by the bandwidth of the AOD.[11] Once the acousto-optic signal is stabilized, the resolution of the output image is limited by the diffraction because of the finite aperture size of the AOD. Along the direction orthogonal to the acoustic signal flow the output image quality is limited by the aperture height of the AOD, irrespective of time–bandwidth product. In this way an image can be continuously shifted rapidly, while high resolution is preserved. Such an elegant method of fast image shift may have been proposed in the past for different appli-

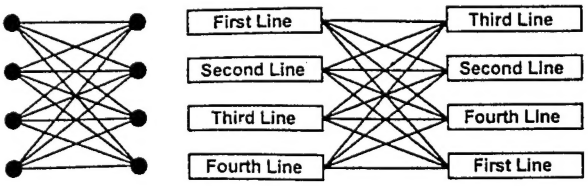

Fig. 1. Interconnection links for (a) conventional point-to-point and (b) block-to-block communications. Each block contains time-varying two-dimensional spatial information.

0146-9592/95/181904-03$6.00/0

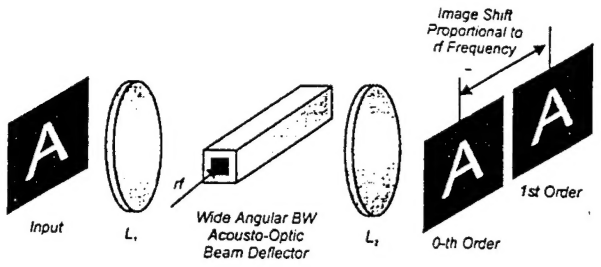

Fig. 2. Fast image shift obtained with an acousto-optic beam deflector.

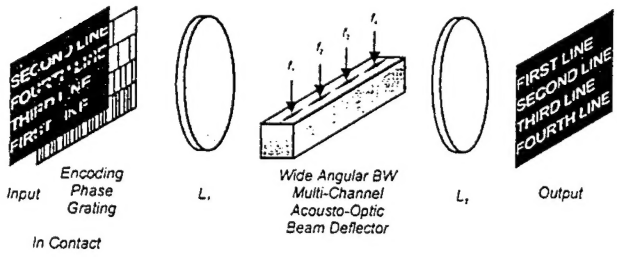

Fig. 3. Fast reconfigurable image switching/routing system.

cations. However, to our knowledge it has rarely been used in a system.[12]

Figure 3 shows our approach to obtaining arbitrary image crossbar/shuffling based on the fast image shift technique explained above. Because each block needs to be shifted independently, the system shown in Fig. 2 needs to be multiplexed somehow. To ensure efficient multiplexing, we defined each block and encoded it by its own spatial frequency, using an array of phase gratings that is in close contact with the input. The light signal, modulated spatially by its own grating, is focused to the corresponding channel of the multichannel AOD and is deflected independently to the desired direction to form a suitably shifted image at the output plane. In this way, an arbitrary configuration can rapidly be obtained by simple adjustment of the rf applied to each of the multichannel AOD's.

Because of the high light throughput and the low coherence requirement of the system that does not involve any hologram recording process, a compact two-lens system with a low-power laser diode may be implemented. Also, arbitrary block definition, including two-dimensional input–output topologies, is possible. The topology can also be reconfigured with two-dimensional spatial light modulator instead of a fixed grating mask.

The first and most important requirement of the AOD for this application is large angular bandwidth because the light incoming to the AOD spans a certain angular range. This large angular bandwidth may be achieved by use of an anisotropic property of the acousto-optic material. However, in this experiment the wide angular bandwidth is obtained primarily by use of a relatively thin (0.45-mm) transducer along the light-propagation direction to reduce the interaction length while preserving high-Q factor. The four-channel AOD with wide angular bandwidth was fabricated by a Newport Electro-Optical Systems model N45100-4CH multichannel acousto-optic beam deflector. The device has a wide angular bandwidth of 102 mrad and 633 nm. The active material of the AOD is shear mode tellurim dioxide, which permits large acousto-optic beam deflection because of the slow speed of the acoustic wave in the material. Also, the high acousto-optic figure of merit of the material gives high diffraction efficiency without the need for an excessively long interaction length, which could limit the input field of view. The operating rf ranges from 75 to 125 MHz, and the maximum diffraction efficiency is ~75% at center frequency, 100 MHz. The size of the whole multichannel AOD is 10 mm (along the acoustic path) × 8 mm (along the optical path) × 31 mm (along the channel direction). Four transducers are arranged along the channel direction, and each transducer has a diamond shape with the dimensions 0.45 mm (along the optical path) × 5.75 mm (transverse to the optical path), as shown in Fig. 3. The center-to-center spacing of the multichannel AOD is 6.75 mm, and the usable acoustic beam width is 3.5 mm.

The phase mask used in this experiment is designed to satisfy the following requirements: First, the first-order diffraction components of interest need to be separated from undesirable higher-order diffraction components. Second, the size and separation of the Fourier spectra should match those of the multichannel AOD to avoid cross talk. The size of each spectrum should just fill the acoustic aperture to preserve high spatial frequency while preventing cross talk from adjacent channels. Also, there is a trade-off between resolution and aberration of output images. For a given multichannel AOD, increasing the focal length of lens L_1 increases the size of each spectrum and the separation between the spectra and reduces the maximum spatial frequency through the device. On the other hand, using a shorter-focal-length lens in the system can cause larger off-axis aberrations.

To avoid higher-order diffraction, one may consider holographic sinusoidal gratings. However, in this experiment we fabricated an array of rectangular gratings, using an electron beam machine for easier control of frequencies and block definitions. Instead, the frequencies of the multiple gratings were biased so that the lowest second-order frequency was greater than the highest first-order frequency plus twice the spatial bandwidth of the data image.

One might consider a volume holographic grating array to increase light efficiency. However, the problem with the volume grating is the loss in spatial frequency components that is due to the phase-matching selection property. An alternative way to increase light efficiency would be to use an array of ruled gratings or microwedge prisms. In this way, one can achieve encoding without losing light. Also, the phase gratings can be recorded on a spatial light modulator such as a liquid-crystal television for programmable block definition and encoding. In this case care must be taken to ensure close contact between the input transparency and the phase mask. If close contact is not achievable because of other constraints, telescopic imaging optics can be used to image the input onto the phase mask, sacrificing the compactness of the system.

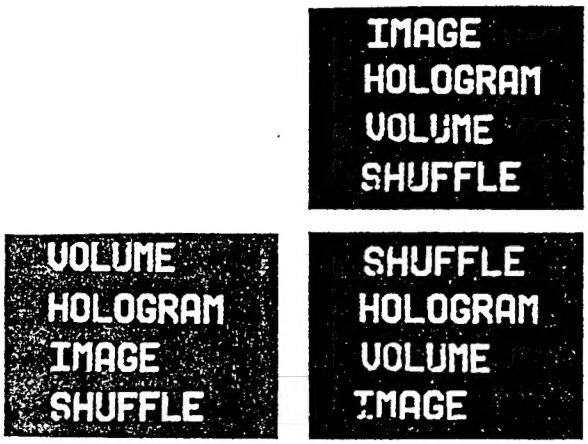

Fig. 4. Experimental results of 4 by 4 image switching/routing: (a) input image, (b) examples of shuffled output images.

A 5-mW He–Ne laser is used as a light source in this experiment. The input and the encoding masks are fabricated with an *e*-beam machine, and the two are attached to each other. The input is 6 mm high and is divided into four blocks along the vertical direction. The frequencies of the encoding gratings are 140, 180, 220, and 260 lines/mm. We chose these numbers carefully after considering the requirements explained above. The focal length of lens L_1 is 26 cm. The size of each spectrum for the input with the maximum spatial frequency of 10 lines/mm is ~3.2 mm, which is smaller than the acoustic beam width of 3.5 mm.

Figure 4 shows the experimental results. Figure 4(a) shows the original input image, and Fig. 4(b) shows various shuffled images obtained from the system. This figure demonstrates the arbitrary interconnection capability of the system. As the figure shows, output images with high resolution can readily be obtained.

In a separate experiment a real-time crossbar/shuffling of images was demonstrated for four channels. The frequencies applied to each of the multichannel AOD's can be varied by four frequency synthesizers controlled by a computer in less than 1 μs. In this way fast image crossbar switching in microsecond intervals was demonstrated.

In conclusion, we have proposed and demonstrated a novel image crossbar/shuffling system that can be reconfigured within a few microseconds. Because of high light efficiency, low coherence requirements, and simple configuration, the system can be made compact and robust. The system can be used in a variety of applications such as switching/routing and sorting of high-speed images.

This research was supported by the U.S. Air Force, Rome Laboratories. E. G. Paek was at Rockwell Science Center while this work was performed.

References

1. J. Midwindter, *Photonics in Switching* (Academic, San Diego, Calif., 1993).
2. F. Mok, M. C. Tackitt, and H. M. Stoll, Opt. Lett. **16,** 605 (1991).
3. D. Psaltis and N. H. Farhat, presented at the ICO-13 Conference, Sapporo, Japan, 1984.
4. C. Warde and J. Kottas, Appl. Opt. **25,** 940 (1986).
5. H. S. Stone, IEEE Trans. Comput. **C-20,** 153 (1971).
6. K-H. Brenner and A. Huang, Appl. Opt. **27,** 135 (1988).
7. G. E. Lohman and A. W. Lohmann, Opt. Eng. **27,** 893 (1988).
8. N. Davidson, A. A. Friesem, and E. Hasman, Appl. Opt. **31,** 1810 (1992).
9. M. W. Haney and J. J. Levy, Appl. Opt. **30,** 2833 (1991).
10. For example, see A. Marrakchi, ed., special issue on photonic switching and interconnects, Opt. Eng. **29**(3) (1990).
11. R. J. Collier, C. B. Burckhardt, and L. H. Lin, *Optical Holography* (Academic, New York, 1971), App. III, p. 590.
12. Y. Shi, Opt. Acta **33,** 895 (1986).

*U.S. GOVERNMENT PRINTING OFFICE: 1996-710-126-20167

MISSION

OF

ROME LABORATORY

Mission. The mission of Rome Laboratory is to advance the science and technologies of command, control, communications and intelligence and to transition them into systems to meet customer needs. To achieve this, Rome Lab:

a. Conducts vigorous research, development and test programs in all applicable technologies;

b. Transitions technology to current and future systems to improve operational capability, readiness, and supportability;

c. Provides a full range of technical support to Air Force Materiel Command product centers and other Air Force organizations;

d. Promotes transfer of technology to the private sector;

e. Maintains leading edge technological expertise in the areas of surveillance, communications, command and control, intelligence, reliability science, electro-magnetic technology, photonics, signal processing, and computational science.

The thrust areas of technical competence include: Surveillance, Communications, Command and Control, Intelligence, Signal Processing, Computer Science and Technology, Electromagnetic Technology, Photonics and Reliability Sciences.